Next Generation HDI Technologies for Magnetic Hard Disks

Mitsuo Kobayashi
Michinari Kamiyama
Akiyasu Kumagai

1. Introduction

With enhanced recording density of magnetic hard disk drives (HDDs), requirements for reducing the "magnetic spacing", the distance between the read-write head and the magnetic layer, are becoming more and more critical. In order to reduce magnetic spacing, the most effective means is to reduce flying height of the head. Following current trends, the flying height will decrease below 20nm and various demands are being placed on the hard disk (hereinafter referred to as the disk) (Fig. 1).

From this viewpoint, development in various fields is being actively promoted in order to define the phenomena involved in the head disk interface (HDI), that is, interactions between the head and disk. Problems with HDI technology have become increasingly important together with reliability improvement of a hard disk drive.

2. Problems of HDI Technology Related to the Disk

Firstly, to reduce substantially the magnetic spacing, it is strongly required that the disk has both a thinner carbon overcoat layer, covering the surface of the magnetic layer, and a thinner lubricant layer on top. Furthermore, the surface roughness (R_a) and the surface undulation (waviness) (W_a) of the disk must be made small so that the surface will not come in contact with the head, even if the head flying height is reduced. Precise substrate processing techniques to obtain a flat and smooth surface have become more critical.

Secondly, another problem is the contact of the head and disk that necessarily occurs during starts and stops. In the current CSS (contact start stop) system broadly used, the laser bump system is applied as means to make the contact area as small as possible. The development of design and processing techniques for a laser bumps of smaller diameter and high density has been accelerated, keeping pace with the reduction in magnetic spacing.

On the other hand, there is a demand for a disk design able to withstand temporary contact of the head in a load-unload system, which will broadly be used in future.

Fig.1 Cross section of flying head and hard disk

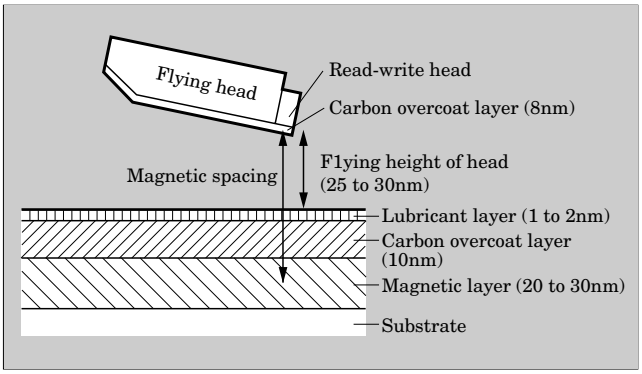

In this paper, we suggest a fabrication method for the CVD (chemical vapor deposition) carbon overcoat layer, and discuss the analysis technology to microscopically observe this layer and the distribution of the lubricant used.

3. CVD Overcoat Layer

3.1 CVD and carbon layer characteristics

At present, the carbon overcoat layer is deposited by sputtering a graphite target. If the layer is not more than 10nm thick, it is likely to be defective with regard to durability or corrosion-resistance for protection. A layer formed by CVD has superior coverage characteristics and protective performance for under layers because the layer formation is accompanied by a surface chemical reaction. Because the layer material of carbon can be controlled with ion energy, compared with a sputtered layer, a finer and more rigid layer can be formed. Accordingly, fabrication of the carbon overcoat layer will employ the CVD method in the future.

Among CVD applications, filament type ion beam deposition (IBD), hollow cathode type ion beam deposition, ECR (e1ectron cyclotron resonance)-CVD and RF (radio frequency)-CVD are currently suggested for applications to disk. The carbon overcoat layer and

Fig.2 Principle of ECR-CVD

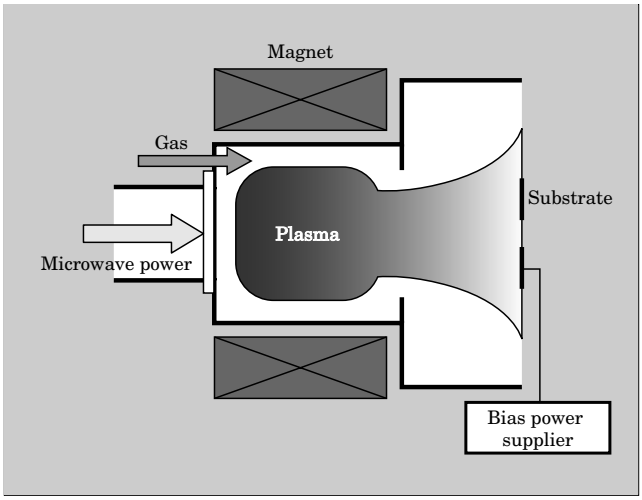

Fig.3 Result of Raman spectroscopy measurement

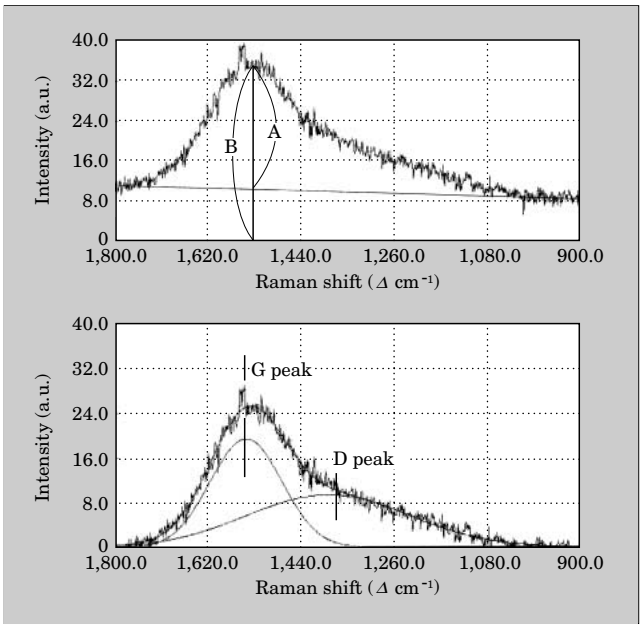

related equipment of ECR-CVD, IBD and RF-CVD have already been evaluated. Hollow cathode type ion beam deposition will be evaluated in the future. This paper describes layer deposited by ECR-CVD and IBD in particular.

3.2 Carbon overcoat layer by ECR-CVD

When microwaves of 2.45GHz are introduced into a magnetic field of 875 G, electron cyclotron resonance occurs, converting the microwave energy into kinetic energy with high efficiency, and high-density plasma is formed. ECR-CVD utilizes this principle as shown in Fig. 2. The same structure is arranged also on the opposite side of substrate and microwaves are introduced differing in phase angle by 90° so as to prevent interference.

Raman scattering spectroscopy is generally used to evaluate the carbon layer material. Figure 3 shows a

Fig.4 Process dependence of B/A characteristic (ECR-CVD)

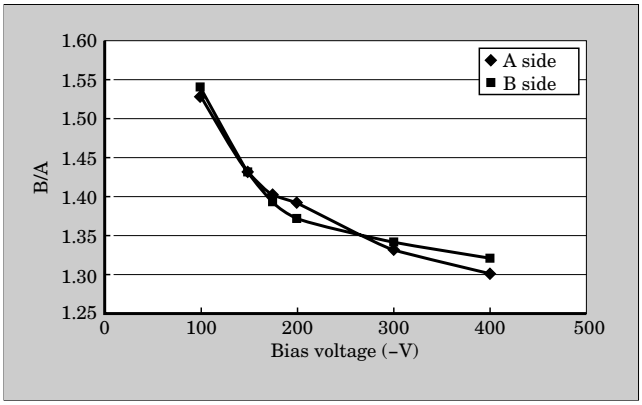

Raman spectrum for the case where a carbon layer has been deposited with C_2H_4 of 0.03 SLM, microwave power of 70W, and a bias voltage of – 200V. We observed the carbon layer, exciting it with an Ar laser light of 514nm. A peak known as the D-peak appears near 1,350cm^{-1}, possibly inherent in the carbon on the border of a graphite crystallite. Another peak known as the G-peak appears near 1,570cm^{-1}, inherent in the planar vibration of the graphite. Both peaks superimpose on the broadband fluorescent component having a peak at approximately 3,000cm^{-1}. As shown in Fig. 3, we assume the total intensity of G-peak to be B. Subtracting the intensity of the fluorescent component from B, we assume this intensity to be A. The intensity ratio B/A correlates with the hydrogen concentration in the carbon layer. We know that if the ratio B/A increases, the hydrogen concentration in the carbon layer becomes higher.

Among the deposition parameters such as microwave power, flow rate of raw material gas (ethylene: C_2H_4), bias voltage applied on the substrate, etc., the parameter most influential on the layer material is the bias voltage applied on the substrate. Figure 4 shows the bias voltage dependence of the ratio B/A characteristic obtained by Raman scattering spectroscopy measurement. As the negative bias voltage increases, the ratio B/A becomes smaller, the hydrogen concentration in the layer decreases, and the layer goes finer. It is believed that the impact energy of ions becomes larger with increasing bias voltage, and as a result, weakly combined hydrogen atoms are separated and carbon atoms are rearranged in the layer.

3.3 Carbon layer by IBD

The principle of IBD equipment is shown in Fig. 5. Thermoelectrons are emitted from a heated filament and attracted to an anode electrode. They collide with raw material gas flowing from the anode side and ionize. The ionized gas is repelled by the anode voltage and attracted by the negative bias voltage applied on the substrate. The ionized gas arrives at the substrate to form the layer. Similar to ECR, IBD controls the carbon layer material with a voltage applied on the

Fig.5 Principle of IBD-CVD

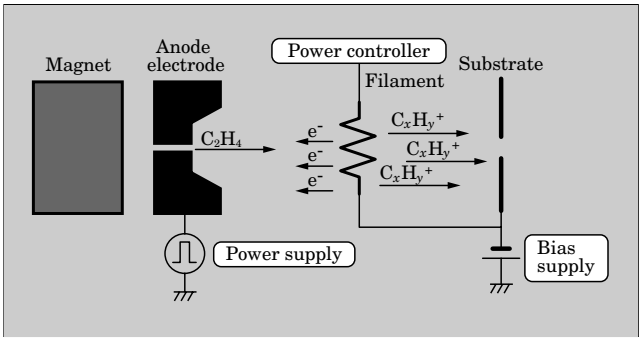

Fig.6 Process dependence of B/A characteristic

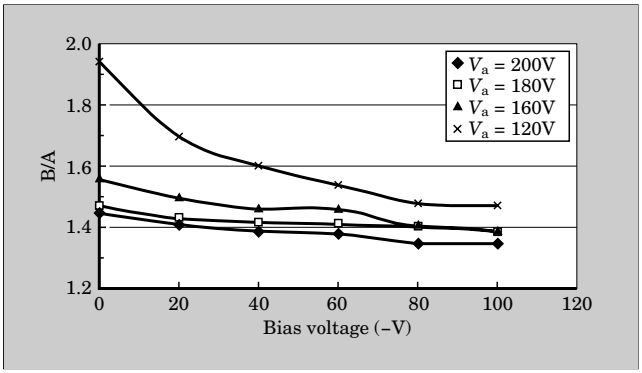

substrate.

IBD in particular controls the layer material with the sum of the absolute values of the anode voltage and bias voltage. With the anode voltage (V_a) as a parameter, the dependency of the ratio B/A upon the bias voltage applied on the substrate is shown in Fig. 6. As in the case of ECR, the ratio B/A decreases as the bias voltage increases. However, as the anode voltage becomes higher, its effect on the bias voltage becomes smaller and the ratio B/A converges to approximately 1.4. If the anode voltage is higher, the initial energy of the ions becomes larger and therefore the effect of the bias voltage is barely noticeable.

At first, we thought it possible to develop a method to deposit a layer on an insulating substrate without applying a bias voltage and increasing the anode voltage. However, unless a bias voltage is applied, the ions repelled by the anode voltage spring toward the space around the substrate. In other words, the same material as deposited on the substrate is deposited on many places in the chamber. This deposited material has a relatively high internal stress, and if made thick, will exfoliate to create particles. We determined that this process could not be applied to mass production. By lowering the anode voltage and applying a bias voltage on the substrate, we utilized a fabrication process capable of suppressing particle scatter by attracting the ions to the substrate.

3.4 Characteristics of the CVD layer

We evaluated the durability of the carbon overcoat layer by a CSS test that repeats starts and stops. In addition to the CSS test, we investigated the performance of the carbon overcoat layer and the resistance of the layer surface against gas adsorption in order to secure high reliability.

Fig.7 Co separation versus carbon layer thickness

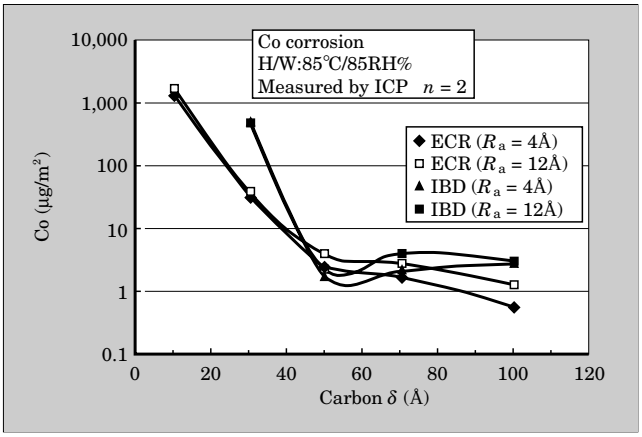

For the coating performance, we applied a method to investigate the amount of cobalt (Co), the main material of the magnetic layer, that corrodes the disk in a high temperature and humidity environment. According to the result shown in Fig. 7, ECR and IBD do not differ much in coating performance for layer thicknesses of 5nm or more, but ECR seems superior for layer thicknesses of 5nm or less. Supposedly, IBD deposits the layer mainly by ions, but ECR forms the layer with a surface reaction of neutral radicals.

In addition, we measured and evaluated the resistance of the layer surface against gas contamination with time-of-flight secondary ion mass spectroscopy (TOF-SIMS) after leaving it for 24 hours in atmospheres of SO_2 gas of 0.1ppm concentration and NH_3 gas of 1ppm concentration. When acid gas SO_2 is adsorbed, the ions of sulfuric acid cause Co corrosion of the magnetic layer. When alkaline gas NH_3 is adsorbed, the ammonium ions cause the head to become dirty.

CVD carbon layers will become, without a doubt, the mainstream of protective overcoats in the future due to their superior performance in fineness and surface coating. However, many unresolved issues such as long term stability of the fabrication equipment, particle scattering and related suppressing methods need to find solutions as quickly as possible. We will aggressively promote further development aiming at the highest technical levels.

4. Observation Techniques of High Space Resolution for Liquid Lubricant

Analysis techniques that provide much chemical information, such as Fourier transform infrared spectroscopy (FTIR), X-ray photoelectron spectroscopy (XPS) and time-of-flight secondary ion mass spectrom-

Fig.8 Principle of liquid lubricant thickness evaluation by SPM

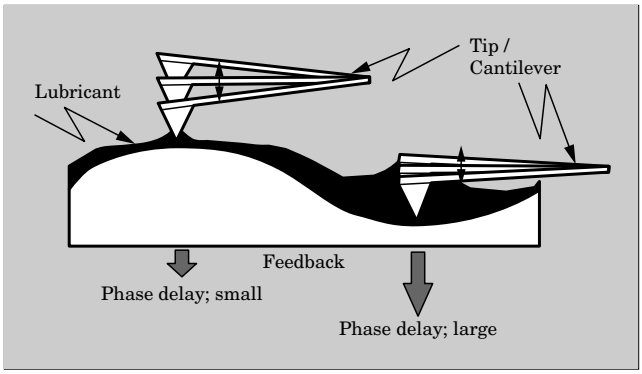

Fig.9 Distribution of liquid lubricant on disk

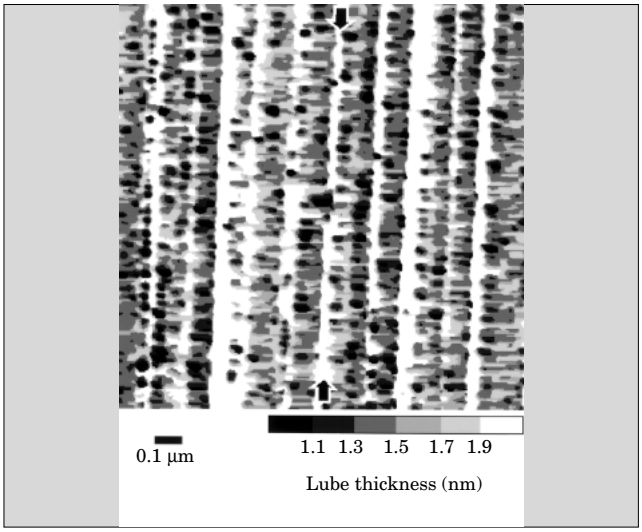

etry (TOF-SIMS), are utilized to investigate extremely thin layers (several nm or less) of a liquid lubricant placed on the disk media. It is not easy, however, for the aforementioned techniques to evaluate the distribution of lubricant at high spatial resolutions that do not exceed the sub-micron level.

The tribology between the head and disk should naturally be discussed from a microscopic viewpoint. Therefore, we have developed a new method to evaluate liquid lubricant distribution utilizing a scanning probe microscope (SPM) that sensitively evaluates the sample surface at a high spatial resolution.

4.1 Principles

SPM is the general term for analysis techniques to investigate the surface state of a sample by detecting interactions between the surface and a sharpened tip.

The probe used is fabricated by silicon micromachining and is integrated into the edge of a cantilever. While vibrating the cantilever at a frequency near the resonance frequency, the sample of the disk media surface is brought close to the probe. At the position where it touches the probe, the vibration amplitude of the probe decreases due to the meniscus force of lubricant. Then, SPM works by feedback to move the sample away from the probe until the original vibration amplitude is restored. When the probe is peeled away from the lubricant, a phase delay occurs in the vibration of the cantilever due to viscosity of the lubricant. We can observe the thickness distribution of the lubricant layer by monitoring this phase delay (see Fig. 8).

The phase imaging mode itself is a well-known method to detect phase. We applied this technique to the lubricant of the disk and developed a new evaluation method that could quantitatively measure thickness distribution of the liquid lubricant layer at high space resolution.

4.2 Results

When we observed the lubricant layer of the disk with the above-mentioned method, we found that the phase delay did not continuously change with the local distribution of lubricant layer thickness. In the local area of observation, where the lubricant layer thickness exceeds a certain threshold value, the probe becomes suddenly trapped in the lubricant layer and produces a large phase delay.

In other words, the phase image is displayed as a binary figure, clearly separating the thick and thin parts of the lubricant layer. We also found that we could control the threshold value with the vibration amplitude of the cantilever. By superimposing phase images of different vibration amplitudes, we can obtain a topological image of the liquid lubricant layer's thickness.

Based on the data thus provided, we can calculate the volume of the liquid lubricant in the area of observation. The calculated volume is only a relative quantity of lubricant, because thickness of the lubricant layer is given by the vibration amplitude of the cantilever as a quantity proportional to the layer thickness. However, the volume has a close correlation with the average quantity of lubricant evaluated by other techniques (FTIR, etc.) and we consider that this method can quantitatively evaluate the distribution of liquid lubricant.

By comparing the relative quantity of lubricant obtained by this method with the average quantity of lubricant measured by the other techniques, we can convert the vibration amplitude of the cantilever into the thickness of the lubricant layer.

Figure 9 shows a distribution of liquid lubricant on Al substrate disk evaluated by the above-mentioned method (overcoat layer; a-C:H:N). A brighter color indicates a thicker lubricant layer.

In this technique, the vibration amplitude of the cantilever is gradually increased until finally the probe becomes untrapped in the area of observation, and the shape of the disk itself can be seen by using atomic force microscope mode. In other words, the disk surface image can be compared with the lubricant distribution.

In Fig. 9, the area between two arrows is a textured groove. We understand that, in this disk , lubricant is thick at the bottom of the groove and thin at the slope of the groove. Definition of correct spatial resolution may be difficult, but lubricant structures on the order of approximately 10nm can be observed. The spatial resolution that can be observed is enhanced by approximately two digits compared with conventional techniques.

We will be able to use this technique as an analysis tool for microscopic phenomena involved in the head and disk interface in future.

5. Conclusions

As examples of HDI technology, we described the latest fabrication methods of the CVD carbon overcoat layer and observation techniques of the CVD carbon overcoat layer and related lubricant distribution. HDI technology involves a wide range of technical fields. To enhance the level of these important techniques in securing reliable HDDs, we will continue to tackle further development in these fields.